ACS APPLIED MATERIALS & INTERFACES

Research Article

www.acsami.org

Layer-by-Layer Self-Assembly of TiO_2 Hierarchical Nanosheets with Exposed {001} Facets As an Effective Bifunctional Layer for Dye-Sensitized Solar Cells

Weiwei Sun,[†] Tao Peng,[†] Yumin Liu,[‡] Wenjing Yu,[†] Kun Zhang,[†] Hadja Fatima Mehnane,[†] Chenghao Bu,[†] Shishang Guo,*[,†] and Xing-Zhong Zhao*[,†]

[†]School of Physics and Technology and Key Laboratory of Artificial Micro- and Nano-structure of Ministry of Education, Wuhan University, Wuhan, 430072, People's Republic of China

[‡]Institute for Interdisciplinary Research (IIR), Jianghan University, Wuhan, 430056, People's Republic of China

ABSTRACT: Layer-by-layer self-assembled TiO_2 hierarchical nanosheets with exposed {001} facets have been successfully fabricated via a simple one-step solvothermal reaction. The anatase TiO_2 layer-by-layer hierarchical nanosheets (TiO_2 LHNs) exhibit favorable light scattering effect and large surface area, owing to their layer-by-layer hierarchical structure. When applied to the dye-sensitized solar cells (DSSCs), the layer-by-layer hierarchical structure with exposed {001} facet could effectively enhance light harvesting and dye adsorption, followed by increasing the photocurrent of DSSCs. As a result, the photoelectric conversion efficiency (η) of 7.70% has been achieved for the DSSCs using TiO_2 LHNs as the bifunctional layer, indicating 21% improvement compared to the pure Degussa P25 (6.37%) as photoanode. Such enhancement can be mainly ascribed to the better light scattering capability of TiO_2 LHNs, higher dye adsorption on TiO_2 LHN {001} facets, and longer lifetime of the injected electrons in TiO_2 LHNs compared to P25, which are examined by UV−vis spectrophotometry and electrochemical impedance spectroscopy under the same conditions. These remarkable properties of TiO_2 LHNs make it a promising candidate as a bifunctional scattering material for DSSCs.

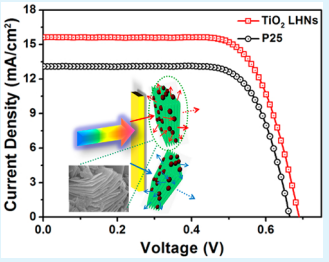

KEYWORDS: *TiO_2 hierarchical nanosheets, exposed {001} facets, favorable light scattering effect, long lifetime, dye-sensitized solar cells*

1. INTRODUCTION

Since the groundbreaking report by O'Regan and Grätzel in 1991, dye-sensitized solar cells (DSSCs) have been considered as a promising low-cost alternative to conventional Si-based photovoltaic devices.[1,2] To date, a new milestone of power conversion efficiency of more than 12% has been achieved using a cobalt complex based redox mediator in conjunction with zinc porphyrin dye as sensitizer.[3]

As an important component of DSSCs, various metal oxide materials have been used as photoanode materials to develop high performance DSSCs, such as TiO_2, ZnO, SnO_2, etc.[4,5] Among them, mesoporous TiO_2 film exhibits the highest power conversion efficiency in DSSCs. Various methods have been used to synthesize nanostructured TiO_2.[6−10] Specifically, sol−gel chemistry is a very fruitful routes to prepare TiO_2 nanostructures for application in DSSCs.[11,12] Unfortunately, as is well-known, the scattering efficiency of the TiO_2 nanoparticle is so weak that a large part of the sunlight cannot be absorbed by the sensitizer when it penetrates the films. In order to achieve these objectives, much effort has been devoted to explore new methods to improve the light harvesting efficiency.[13−18] In addition to exploiting a new efficient sensitizer, it has been confirmed that introducing a scattering layer into a photoanode is an efficient approach to enhance light harvesting efficiency and power conversion efficiency.[19,20] However, the introduction of larger size scattering particles often inevitably leads to a decrease of the surface area and the dye absorption, which offsets the improvement of light harvesting efficiency.[20] In order to solve this problem, a hierarchical mesoporous TiO_2 microsphere which consists of the aggregation of small TiO_2 nanocrystallines was adopted as a new scatterer with double function.[21] These hierarchical TiO_2 microspheres show an efficient scattering effect and maintain a high dye absorption ability at the same time. However, the synthesis of those hierarchical mesoporous microspheres involves a time-consuming process.

At the same time, the anatase TiO_2 crystalline with an exposed {001} surface can absorb more dye molecules, which is supported by theoretical and experimental results.[22−26] As a consequence, this type of TiO_2 has superior application in the photoanode of DSSCs. The incorporation of large size anatase TiO_2 nanocrystalline with exposed (001) facets in the photoanode can not only enhance the scattering effect but also improve dye molecule absorption, both are beneficial to the sunlight capture and utilization.

Received: February 28, 2014
Accepted: June 2, 2014
Published: June 2, 2014

Here, we report a simple method to synthesize the hierarchical layer-by-layer self-assembled TiO_2 nanosheets with dominated {001} facets by a one-step hydrothemal process. To the best of our knowledge, this is the first time to apply this new type of anatase TiO_2 layer-by-layer hierarchical nanosheets with dominant {001} facets (denoted as TiO_2 LHNs) as the dual-functional scattering layer in DSSCs. It has been confirmed that it possesses both excellent light scattering properties and dye adsorption ability. When the photoanode is based on the TiO_2 LHNs as the bifunctional scattering top layer and commercial P25 nanocrystallines as the bottom layer, a power conversion efficiency of 7.7% has been achieved, which is about 21% higher than that of the photoanode based on the commercial P25 (6.37%) under the same conditions. A proposed schematic diagram for the configuration of DSSCs assembled using TiO_2 LHNs as the dual-functional scattering layer is shown in Scheme 1.

Scheme 1. DSSCs Photoanode Assembled Using TiO_2 LHNs as the Bifunction Layer

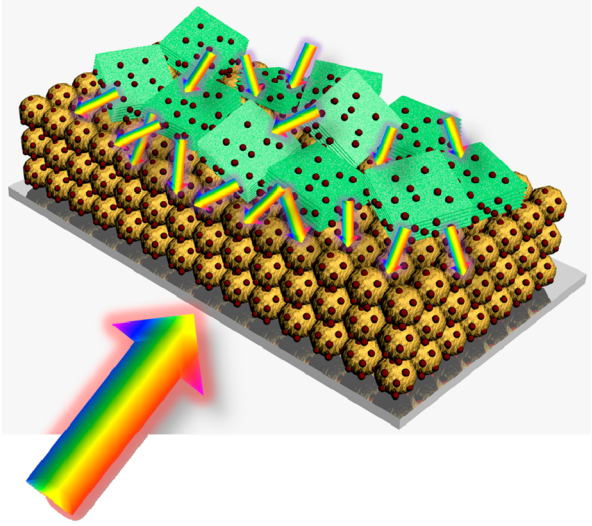

2. EXPERIMENTAL SECTION

2.1. Material Synthesis. Anatase TiO_2 LHNs with exposed {001} facets were prepared according to a previous report.[27] In a typical experiment, we mixed titanium tetrafluoride (0.20 g) in 80 mL of benzyl alcohol until we obtained a homogeneous solution under continuous magnetic stirring for about 4 h. Then, the mixed solution was transferred to a Teflon-lined stainless steel autoclave of 100 mL capacity and heated for 24 h at 160 °C. Finally, the white, crystalline titania powder was collected by centrifugation, washed with ethanol, and then dried in vacuum at 80 °C.

2.2. Fabrication of DSSCs. For preparation of the TiO_2 LHNs paste, 0.9 g of the prepared TiO_2 LHNs powder was added to the solution containing ethanol (4 mL), water (1 mL), and acetylacetone (0.16 mL) and then stirred for 2–3 h. The TiO_2 P25 paste was prepared by a ball-milling process. A doctor-blade method was used to prepare photoelectrodes, followed by sintering at 500 °C for 30 min. For dye adsorption, the TiO_2 photoanode was immersed in a 0.5 mM N719 ethanol solution and heated at 60 °C for 12 h, then rinsed with ethanol and dried. The liquid electrolyte was prepared by blending 1 M PMII(1-methyl-3-propyl imidazolium iodide), 0.04 M LiI, 0.03 M I_2, 0.1 M GuSCN(guanidinium thiocyanate), 0.5 M TBP(4-*tert*-butylpyridine) in acetonitrile and propylene carbonate (v/v = 1:1) between them. The Pt counter electrode was prepared by depositing a thin layer of Pt on FTO by magnetron sputtering.

2.3. Characterization. X-ray diffraction (XRD) characterization was performed on a D8 Focus diffractometer. Field emission scanning electron microscopy, FE-SEM (Sirion FEG) was applied to study the morphology and structure of the as-prepared samples. TEM and HRTEM investigations were carried out using a JEOL 2010, equipped with an energy dispersive X-ray analysis (EDX) system. The specific surface area and pore size distribution of as-prepared samples were investigated by Brunauer–Emmet–Teller (BET) nitrogen sorption–desorption measurement (Quantachrome NOVA 4200e). To obtain the dye loading amount adsorbed on different photoanodes, NaOH aqueous solution (0.1 M) was used for desorption and UV–vis spectrometer (Varian Carry 5000) was used to measure the absorption spectra. Diffuse reflection spectra of the films were observed on Carry 5000. The photocurrent–voltage characteristics of the cells were recorded by applying external potential bias to the device under AM 1.5 simulated illumination (Newport, 91192) with a power density of 100 mW cm^{-2}, which was calibrated by a Si photodiode, and the active area was controlled by a 0.25 cm^2 mask. Electrochemical impedance spectroscopy (EIS) measurements were also performed on CHI 660C with the frequency ranging from 100 kHz to 0.1 Hz under the open-circuit voltage in the illumination.

3. RESULTS AND DISCUSSION

The typical X-ray diffraction (XRD) pattern of as-synthesized TiO_2 LHNs was measured, as shown in Figure 1. All the sharp

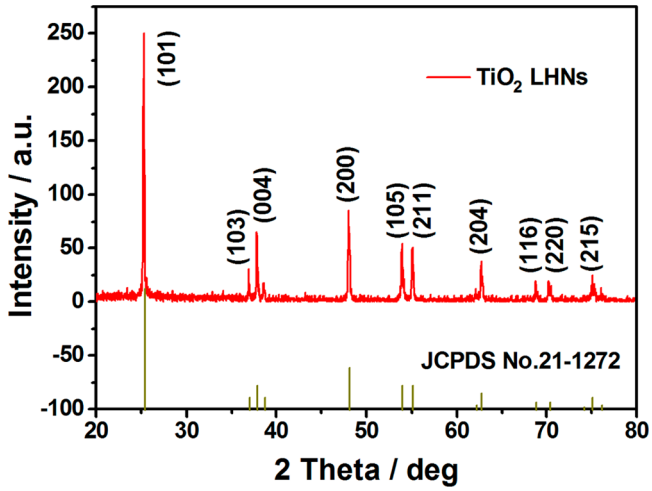

Figure 1. XRD pattern of the as-synthesized TiO_2 LHNs powder.

peaks are in good agreement with the standard data of anatase TiO_2 (JCPDS card no. 21-1272), indicating that the sample is highly crystalline and can be well assigned to the pure tetragonal phase anatase structure without any impurity phase.

The morphology and structure of the as-obtained TiO_2 LHNs was characterized by field-emission scanning electron microscope (FE-SEM) and transmission electron microscope (TEM) as shown in Figure 2. A top view of the TiO_2 LHNs in FE-SEM (Figure 2a) reveals that they are rectangles with edge lengths ranging from about 300 to 400 nm. Figure 2b shows the tilted view of TiO_2 LHNs, which displays that the TiO_2 nanosheets have a highly ordered arrangement with all the nanosheets oriented parallel to each other. TEM image from the side face of the TiO_2 LHNs confirmed that the well-defined layer-by-layer structures and the thickness of an individual TiO_2 nanosheet was only about 6 nm (Figure 2c). Figure 2d shows a high-resolution TEM image recorded from Figure 2c, which evidently showed that the lattice spacing parallel to the top and bottom facets was ~0.24 nm, corresponding to the (001)

dx.doi.org/10.1021/am501233q | ACS Appl. Mater. Interfaces 2014, 6, 9144–9149

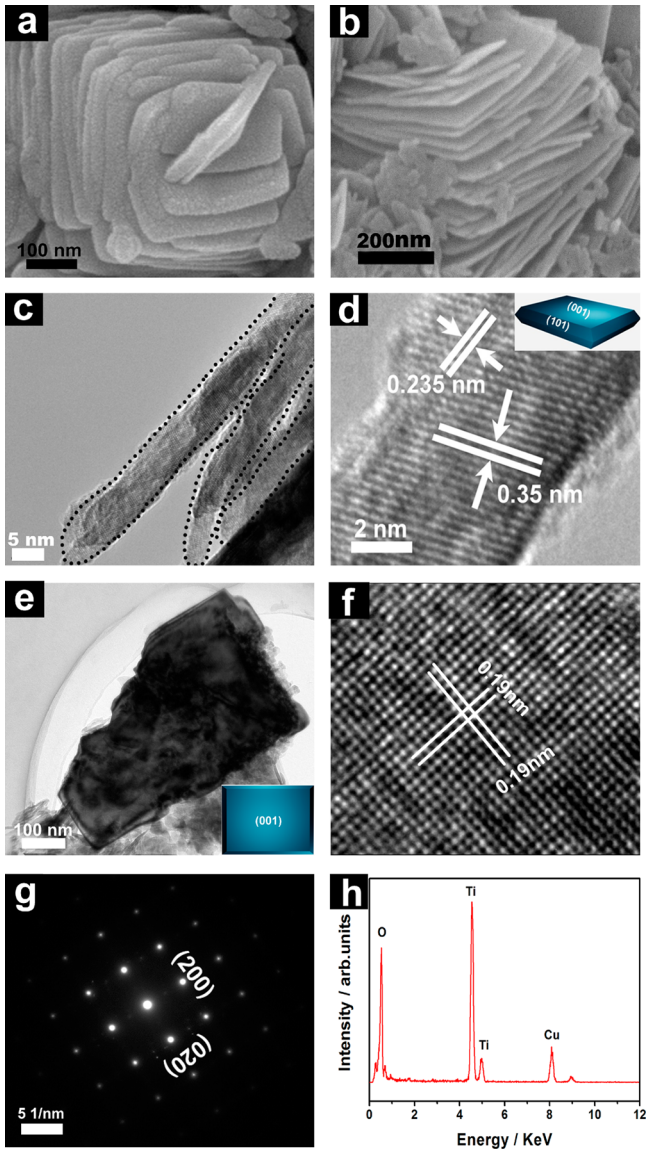

Figure 2. (a) The top view and (b) tilted-view SEM images of the as-synthesized TiO_2 LHNs; (c) TEM images of self-assembling anatase TiO_2 LHNs; (d) HR-TEM images recorded around the edge of the TiO_2 LHNs; (e) TEM image of an individual TiO_2 nanosheet; (f–g) HR-TEM image and the corresponding SAED pattern recorded from and (h) EDX analysis of the anatase TiO_2 LHNs.

planes of anatase TiO_2. On the basis of the above results, the percentage of exposed highly reactive (001) facets on the TiO_2 LHNs was estimated to be over 90%. A top view of the nanosheets in the TEM (Figure 2e) further confirmed that they were rectangles with edge length range from about 300 to 400 nm. The high resolution TEM image in Figure 2f reveals that two sets of lattices are oriented perpendicular to each other with an equal interfringe spacing of 0.19 nm, agreeing well with the spacing of the (200) and (020) lattice planes of anatase-type TiO_2 LHNs. The selected area electron diffraction (SAED) pattern (Figure 2g) reveals that the nanoplates are crystalline with a diffraction pattern of single-crystal anatase along the [001] zone axis, which is in agreement with the HR-TEM image. Further energy-dispersive X-ray analysis (EDX) results confirm the presence of both Ti and O elements in TiO_2 LHNs (Figure 2h).

The porous structure of the TiO_2 LHNs was further investigated with the N2 adsorption/desorption analysis, as shown in Figure 3a. The typical type IV isotherm with a H3 hysteresis loop is visible, indicating a mesoporous structure of as-obtained TiO_2 LHNs.[28] The special surface area obtained from the isotherm is determined to be 78 m^2/g. The Barrett–Joyner–Halenda (BJH) pore size distribution for TiO_2 LHNs is depicted as an inset of Figure 3a. Evidently, the size of most of the pores concentrate is about 28 nm, which is adequate for better penetration of electrolyte in TiO_2 LHNs when used as a bifunctional scattering layer in DSSCs.[29] Figure 3b shows the UV–vis absorption spectrum of the dyes desorbed from the two different photoanodes based on TiO_2 LHNs and P25, respectively, and the calculated amount of the dye adsorbed at the films is listed in Table 1. It can be seen that, an obvious increase in the dye loading amount can be found in TiO_2 LHNs film (1.87×10^{-7} mol cm^{-2}) compared to P25 (1.38×10^{-7} mol cm^{-2}), which is due to the high specific surface area of TiO_2 LHNs, as well as the dominant {001} exposed facets. The possible reflecting and scattering of sunlight in TiO_2 LHN photoanodes is illustrated in Figure 3c, which is favorable to the adsorption of more light for dye molecule. Figure 3d shows the diffuse reflection spectra of the TiO_2 LHNs and P25 photoanodes without dye loading. Comparatively, TiO_2 LHN photoanodes exhibit higher diffuse reflectance in the whole wavelength range from 350 to 800 nm compared to P25. The diffuse reflectance of the P25 film decreases rapidly as the wavelength increases from 410 to 800 nm, due to the small particle size.[30] Whereas, TiO_2 LHN films keep quite high reflectivity in the long wavelength regions, which indicates the better light scattering property in the wavelength of visible light. From the foregoing, the bifunctional TiO_2 LHN photoanodes can not only greatly increase the dye loading rate, but also dramatically improve the light scattering effect, and thus significantly enhance the performance of DSSCs.

The photocurrent–voltage (J–V) characteristics of DSSCs based on TiO_2 LHNs and P25 electrodes were characterized using a mask with an aperture of 0.25 cm^2 at AM 1.5 irradiation of 100 mW cm^{-2}. The typical J–V curves of TiO_2 LHNs and P25 photoanodes are shown in Figure 4a and detailed parameters of the devices are summarized in Table 1. The DSSCs assembled with the TiO_2 LHNs electrode reveals an open-circuit voltage (V_{oc}) of 0.69 V, a short-current density (J_{sc}) of 15.62 mA cm^{-2} and an overall conversion efficiency (η) of 7.70%, whereas DSSCs based on P25 electrode presents a V_{oc} of 0.67 V, a J_{sc} of 13.08 mA cm^{-2} and a η of 6.37%. According to the previous analysis, the enhanced J_{sc} could be attributed to the better dye loading rate and light scattering effect owing to the large specific surface area, dominant {001} facets and distinctive layer-by-layer structure. Besides, V_{oc} of LHNs electrode (0.69 V) is higher than that of P25 (0.67 V), which could be ascribed to the more compact dye molecule absorbed on the {001} facets of LHNs. Densely absorbed and aggregated dye molecules could inhibit tri-iodide ions reaching the surface of TiO_2 LHNs due to steric hindrance, which would greatly decrease the direct recombination of excited and transferred dye electrons with tri-iodide ion.[31] In consequence, a 21% improvement in the overall conversion efficiency was achieved by employing TiO_2 LHN photoanodes compared to pure P25 photoanodes.

To deeply understand the dynamics of electron transport and recombination properties in DSSCs, electrochemical impedance spectroscopy (EIS) was further studied, and the results of

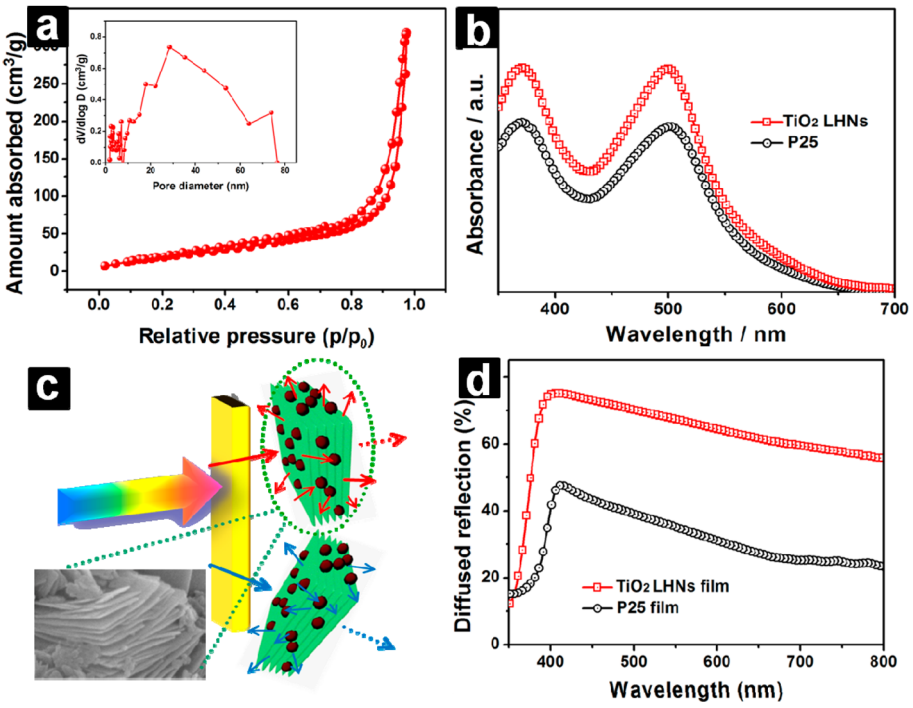

Figure 3. (a) Nitrogen adsorption−desorption isotherm (the inset shows the pore size distributions calculated using the BJH method); (b) UV−vis absorption spectra of the dyes desorbed from the TiO_2 LHNs and P25 films; (c) schematic illustration of the multiple reflecting and scattering of light in the TiO_2 LHNs; and (d) diffuse-reflectance spectra of the films of TiO_2 LHNs and P25.

Table 1. Comparison of Open Circuit Voltage (V_{oc}), Short-Circuit Photocurrent Density (J_{sc}), Fill Factor (FF), Overall Photo-Conversion Efficiency (η) along with the Amount of Adsorbed Dye N719 for the Photoanodes Composed of TiO_2 LHNs and P25, Respectively

electrodes	thickness	V_{oc} (V)	J_{sc} (mA cm^{-2})	FF	PCE (%)	adsorbed dye ($\times 10^{-7}$ mol cm^{-2})
TiO_2 LHNs	13.5 μm	0.69	15.62	0.71	7.70	1.87
P25	13.3 μm	0.67	13.08	0.72	6.37	1.38

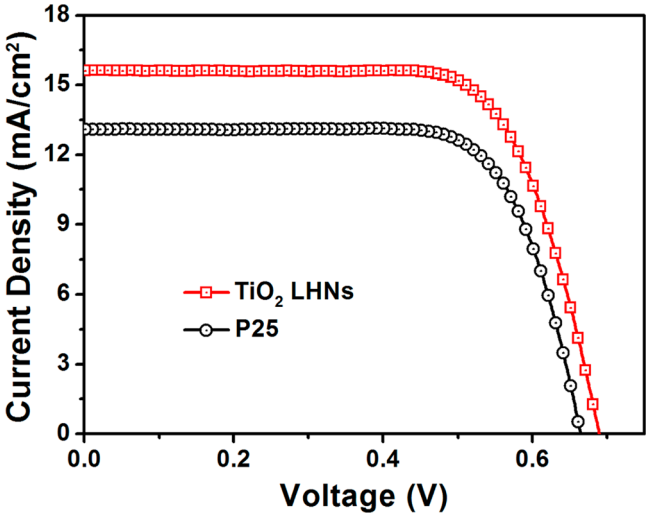

Figure 4. $J-V$ characteristics of the DSSCs with TiO_2 LHNs and P25 photoanodes.

two samples were shown in the Nyquist plots under the open-circuit condition (Figure 5a). In the EIS spectra, two semicircles were observed in the high-frequency region (10^5–10^3 Hz) and in the intermediate frequency region of 10^3–1 Hz, respectively. In accordance with the EIS model reported in the literature, the smaller semicircle in the high-frequency region indicates the electron transport resistance at the counter electrode/electrolyte interface and the larger one represents electron transport and recombination at the photoanode/electrolyte interface.[32,33] The internal impedances were determined by fitting the experimental data with an equivalent circuit containing a total series resistance (R_s), charge-transfer resistance at the Pt/electrolyte interface and at the TiO_2/electrolyte interface, respectively (R_{ct1}, R_{ct2}) and the corresponding constant phase element (CPE_1 and CPE_2) of the device (inset of Figure 5a). The fitted data obtained from EIS analysis are listed in Table 2. It can be noticed that the values of R_s and R_{ct1} for both devices are similar, which is simply because an identical Pt counter electrode was employed for these two devices. However, the values of R_{ct2} shown an obvious difference, which is usually considered to be mainly determined by the charge recombination resistance, with partial contribution from transport resistance.[32] As seen in Table 2, TiO_2 LHNs-based DSSCs show a higher value of R_{ct2} (20.08 Ω) than that of P25 (17.39 Ω), which implies that electron recombination resistance is increased at the TiO_2/electrolyte interface. As mentioned above, this result can be explained by the fact that TiO_2 LHNs process dominant {001} facets, and a densely aggregated dye molecules layer may be formed on the surface of TiO_2 {001} facet, which could inhibit tri-iodide ions from reaching the surface of TiO_2 LHNs and thereby increase

dx.doi.org/10.1021/am501233q | ACS Appl. Mater. Interfaces 2014, 6, 9144−9149

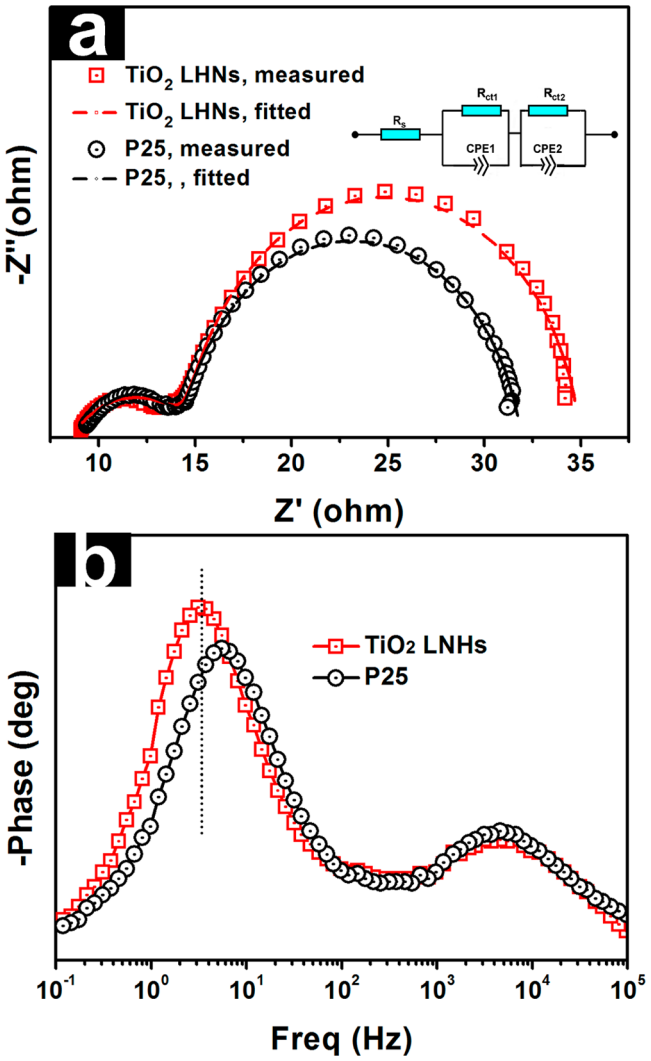

Figure 5. (a) Nyquist plots and (b) the corresponding bode plots of the DSSCs based on TiO_2 LHNs and P25 photoanodes. The inset in (a) displays the equivalent circuit model.

Table 2. EIS Parameters of the DSSCs Determined by Fitting the Experimental Data to the Equivalent Circuit Model

electrodes	R_s	R_{ct1} (Ω)	R_{ct2} (Ω)	f_{max} (Hz)	τ_r (ms)
TiO_2 HFSs	8.59	6.31	20.08	3.09	51.51
P25	9.09	5.43	17.39	5.49	28.99

the recombination resistance as well as the V_{oc} compared to P25. Figure 5b displays the bode phase plots of EIS spectra, containing two main frequency peaks corresponding to the charge transfer process at different interfaces for both of the two photoanodes. It is found that the maximum frequency peak in the intermediate frequency regime, which is related to electron transfer in the TiO_2 LHNs photoanode, is lower than that of the P25 photoanode. The electron lifetime (τ_r) in the DSSCs could be estimated from the following equation:

$$\tau_r = 1/2\pi f_{max}$$

As seen in Table 2, the characteristic frequencies (f_{max}) of the maximum phase shift at the midfrequency peaks were 3.09 and 5.49 Hz for TiO_2 LHNs and P25 photoanodes, respectively. The corresponding τ_r for DSSCs with a TiO_2 LHN photoanode was estimated to be 51.51 ms, which was up to 78% longer than that of the P25 photoanodes (28.99 ms). It can be concluded that the longer electron time implies a lower electron recombination rate, which could slightly heighten the V_{oc} of TiO_2 LHNs compared to P25.[33] These factors are in favor of achieving higher photoelectric conversion efficiency.

4. CONCLUSIONS

In summary, {001} facets exposed anatase TiO_2 nanosheets based on layer-by-layer self-assembled hierarchical structure have been successfully prepared by a simple one-step hydrothermal reaction. Remarkably, the as-prepared TiO_2 LHNs presented outstanding scattering ability and dye loading amount performance due to the large surface area as well as the dominant {001} facets. As a consequence, the DSSCs based on these bifunctional TiO_2 LHNs layers exhibited a significant improvement in the overall power conversion efficiency (7.70%) compared to that of pure P25 photoanode (6.37%). Furthermore, the dynamics studies of EIS revealed that TiO_2 LHN photoanodes with dominant (001) facets possess a longer electron lifetime and therefore lower electron recombination rate compared with P25 photoanodes. This study should provide distinct evidence for the superiority of these novel {001} facet exposed TiO_2 LHN photoanodes for clean energy applications.

AUTHOR INFORMATION

Corresponding Authors

*E-mail: gssyhx@whu.edu.cn.
*E-mail: xzzhao@whu.edu.cn.

Notes

The authors declare no competing financial interest.

ACKNOWLEDGMENTS

This project was funded by the National Basic Research Program (No. 2011CB933300) of China and the National Science Fund for Talent Training in Basic Science (Grant No. J0830310).

REFERENCES

(1) O'Regan, B.; Grätzel, M. A Low-Cost, High-Efficiency Solar Cell Based on Dye-Sensitized Colloidal TiO_2 Films. *Nature* **1991**, *353*, 737−740.
(2) Grätzel, M. Photoelectrochemical Cells. *Nature* **2001**, *414*, 338−344.
(3) Yella, A.; Lee, H.-W.; Tsao, H. N.; Yi, C.; Chandiran, A. K.; Nazeeruddin, M. K.; Diau, E. W.-G.; Yeh, C.-Y.; Zakeeruddin, S. M.; Grätzel, M. Porphyrin-Sensitized Solar Cells with Cobalt (II/III)-Based Redox Electrolyte Exceed 12% Efficiency. *Science* **2011**, *334*, 629−634.
(4) Wu, W.-Q.; Xu, Y.-F.; Su, C.-Y.; Kuang, D.-B. Ultra-Long Anatase TiO_2 Nanowire Arrays with Multi-Layered Configuration on FTO Glass for High-Efficiency Dye-Sensitized Solar Cells. *Energy Environ. Sci.* **2014**, *7*, 644−649.
(5) Ko, S. H.; Lee, D.; Kang, H. W.; Nam, K. H.; Yeo, J. Y.; Hong, S. J.; Grigoropoulos, C. P.; Sung, H. J. Nanoforest of Hydrothermally Grown Hierarchical ZnO Nanowires for a High Efficiency Dye-Sensitized Solar Cell. *Nano Lett.* **2011**, *11*, 666−671.
(6) Rawolle, M.; Sarkar, K.; Niedermeier, M. A.; Schindler, M.; Lellig, P.; Gutmann, J. S.; Moulin, J.-F. o.; Haese-Seiller, M.; Wochnik, A. S.; Scheu, C. Infiltration of Polymer Hole-Conductor into Mesoporous Titania Structures for Solid-State Dye-Sensitized Solar Cells. *ACS Appl. Mater. Interfaces* **2013**, *5*, 719−729.

(7) Kaune, G.; Memesa, M.; Meier, R.; Ruderer, M. A.; Diethert, A.; Roth, S. V.; D'Acunzi, M.; Gutmann, J. S.; Muller-Buschbaum, P. Hierarchically Structured Titania Films Prepared by Polymer/Colloidal Templating. *ACS Appl. Mater. Interfaces* **2009**, *1*, 2862−2869.
(8) Zhang, Y.; Xie, Z.; Wang, J. Supramolecular-Templated Thick Mesoporous Titania Films for Dye-Sensitized Solar Cells: Effect of Morphology on Performance. *ACS Appl. Mater. Interfaces* **2009**, *1*, 2789−2795.
(9) Durupthy, O.; Jeurgens, L. P.; Bill, J. Biomimetic Formation of Titania Thin Films: Effect of Amino Acids on the Deposition Process. *ACS Appl. Mater. Interfaces* **2011**, *3*, 1624−1632.
(10) Violi, I. L.; Perez, M. D.; Fuertes, M. C.; Soler-Illia, G. J. Highly Ordered, Accessible and Nanocrystalline Mesoporous TiO_2 Thin Films on Transparent Conductive Substrates. *ACS Appl. Mater. Interfaces* **2012**, *4*, 4320−4330.
(11) Rawolle, M.; Niedermeier, M. A.; Kaune, G.; Perlich, J.; Lellig, P.; Memesa, M.; Cheng, Y.-J.; Gutmann, J. S.; Müller-Buschbaum, P. Fabrication and Characterization of Nanostructured Titania Films with Integrated Function from Inorganic-Organic Hybrid Materials. *Chem. Soc. Rev.* **2012**, *41*, 5131−5142.
(12) Orilall, M. C.; Wiesner, U. Block Copolymer based Composition and Morphology Control in Nanostructured Hybrid Materials for Energy Conversion and Storage: Solar Cells, Batteries, and Fuel Cells. *Chem. Soc. Rev.* **2011**, *40*, 520−535.
(13) Son, H. J.; Wang, X.; Prasittichai, C.; Jeong, N. C.; Aaltonen, T.; Gordon, R. G.; Hupp, J. T. Glass-Encapsulated Light Harvesters: More Efficient Dye-Sensitized Solar Cells by Deposition of Self-Aligned, Conformal, and Self-Limited Silica Layers. *J. Am. Chem. Soc.* **2012**, *134*, 9537−9540.
(14) Chandiran, A. K.; Comte, P.; Humphry-Baker, R.; Kessler, F.; Yi, C.; Nazeeruddin, M.; Grätzel, M. Evaluating the Critical Thickness of TiO_2 Layer on Insulating Mesoporous Templates for Efficient Current Collection in Dye-Sensitized Solar Cells. *Adv. Funct. Mater.* **2013**, *23*, 2775−2781.
(15) He, Z.; Que, W.; Sun, P.; Ren, J. Double-Layer Electrode Based on TiO_2 Nanotubes Arrays for Enhancing Photovoltaic Properties in Dye-Sensitized Solar Cells. *ACS Appl. Mater. Interfaces* **2013**, *5*, 12779−12783.
(16) Bai, Y.; Xing, Z.; Yu, H.; Li, Z.; Amal, R.; Wang, L. Porous Titania Nanosheet/Nanoparticle Hybrids as Photoanodes for Dye-Sensitized Solar Cells. *ACS Appl. Mater. Interfaces* **2013**, *5*, 12058−12065.
(17) Wang, X.; Sun, L.; Zhang, S.; Wang, X. Ultra-Long, Small Diameter TiO_2 Nanotubes Achieved by an Optimized Two-Step Anodization for Efficient Dye-Sensitized Solar Cells. *ACS Appl. Mater. Interfaces* **2014**, *6*, 1361−1365.
(18) Xie, F.; Cherng, S.-J.; Lu, S.; Chang, Y.-H.; Sha, W. E.; Feng, S.-P.; Chen, C.-M.; Choy, W. C. Functions of Self-Assembled Ultrafine TiO_2 Nanocrystals for High Efficient Dye-Sensitized Solar Cells. *ACS Appl. Mater. Interfaces* **2014**, *6*, 5367−5373.
(19) Dong, Z.; Ren, H.; Hessel, C. M.; Wang, J.; Yu, R.; Jin, Q.; Yang, M.; Hu, Z.; Chen, Y.; Tang, Z. Quintuple-Shelled SnO_2 Hollow Microspheres with Superior Light Scattering for High-Performance Dye-Sensitized Solar Cells. *Adv. Mater.* **2014**, *26*, 905−909.
(20) Li, K.; Xu, J.; Shi, W.; Wang, Y.; Peng, T. Synthesis of Size Controllable and Thermally Stable Rice-Like Brookite Titania and Its Application as a Scattering Layer for Nano-Sized Titania Film-Based Dye-Sensitized Solar Cells. *J. Mater. Chem. A* **2014**, *2*, 1886−1896.
(21) Zhang, Q.; Chou, T. P.; Russo, B.; Jenekhe, S. A.; Cao, G. Aggregation of ZnO Nanocrystallites for High Conversion Efficiency in Dye-Sensitized Solar Cells. *Angew. Chem.* **2008**, *20*, 2436−2440.
(22) Fan, J.; Cai, W.; Yu, J. Adsorption of N719 Dye on Anatase TiO_2 Nanoparticles and Nanosheets with Exposed (001) Facets: Equilibrium, Kinetic, and Thermodynamic Studies. *J. Chem. Asian J.* **2011**, *6*, 2481−2490.
(23) Wu, X.; Chen, Z.; Lu, G. Q. M.; Wang, L. Nanosized Anatase TiO_2 Single Crystals with Tunable Exposed (001) Facets for Enhanced Energy Conversion Efficiency of Dye-Sensitized Solar Cells. *Adv. Funct. Mater.* **2011**, *21*, 4167−4172.
(24) Çakır, D.; Gülseren, O.; Mete, E.; Ellialtıoğlu, Ş. Dye Adsorbates BrPDI, BrGly, and BrAsp on Anatase TiO_2 (001) for Dye-Sensitized Solar Cell Applications. *Phys. Rev. B* **2009**, *80*, 035431.
(25) Fang, W. Q.; Yang, X. H.; Zhu, H.; Li, Z.; Zhao, H.; Yao, X.; Yang, H. G. Yolk@ Shell Anatase TiO_2 Hierarchical Microspheres with Exposed {001} Facets for High-Performance Dye-Sensitized Solar Cells. *J. Mater. Chem.* **2012**, *22*, 22082−22089.
(26) Hengerer, R.; Kavan, L.; Krtil, P.; Grätzel, M. Orientation Dependence of Charge-Transfer Processes on TiO_2 (Anatase) Single Crystals. *J. Electrochem. Soc.* **2000**, *147*, 1467−1472.
(27) Zhu, J.; Wang, J.; Lv, F.; Xiao, S.; Nuckolls, C.; Li, H. Synthesis and Self-Assembly of Photonic Materials from Nanocrystalline Titania Sheets. *J. Am. Chem. Soc.* **2013**, *135*, 4719−4721.
(28) Chen, J. S.; Tan, Y. L.; Li, C. M.; Cheah, Y. L.; Luan, D.; Madhavi, S.; Boey, F. Y. C.; Archer, L. A.; Lou, X. W. Constructing Hierarchical Spheres from Large Ultrathin Anatase TiO_2 Nanosheets with Nearly 100% Exposed (001) Facets for Fast Reversible Lithium Storage. *J. Am. Chem. Soc.* **2010**, *132*, 6124−6130.
(29) Feng, J.; Hong, Y.; Zhang, J.; Wang, P.; Hu, Z.; Wang, Q.; Han, L.; Zhu, Y. Novel Core-Shell TiO_2 Microsphere Scattering Layer for Dye-Sensitized Solar Cells. *J. Mater. Chem. A* **2014**, *2*, 1502−1508.
(30) Zhang, H.; Han, Y.; Liu, X.; Liu, P.; Yu, H.; Zhang, S.; Yao, X.; Zhao, H. Anatase TiO_2 Microspheres with Exposed Mirror-like Plane {001} Facets for High Performance Dye-Sensitized Solar Cells (DSSCs). *Chem. Commun.* **2010**, *46*, 8395−8397.
(31) Ko, K. H.; Lee, Y. C.; Jung, Y. J. Enhanced Efficiency of Dye-Sensitized TiO_2 Solar Cells (DSSC) by Doping of Metal Ions. *J. Colloid Interface Sci.* **2005**, *283*, 482−487.
(32) Sun, W.; Sun, X.; Peng, T.; Liu, Y.; Zhu, H.; Guo, S.; Zhao, X.-Z. A Low Cost Mesoporous Carbon/SnO_2/TiO_2 Nanocomposite Counter Electrode for Dye-Sensitized Solar Cells. *J. Power Sources* **2012**, *201*, 402−407.
(33) Sun, X.; Liu, Y.; Tai, Q.; Chen, B.; Peng, T.; Huang, N.; Xu, S.; Zhao, X. Z. High Efficiency Dye-Sensitized Solar Cells based on a Bi-Layered Photoanode Made of TiO_2 Nanocrystallites and Microspheres with High Thermal Stability. *J. Phys. Chem. C* **2012**, *116*, 11859−11866.